Biointerface Research in Applied Chemistry
Platinum Open Access Journal (ISSN: 2069-5837)

Article
Volume 12, Issue 5, 2022, 6321 - 6335
https://doi.org/10.33263/BRIAC125.63216335

Synthesis and Characterizations of Cu Doped Co_3O_4 Nanostructured Thin Films Using Spray Pyrolysis for Glucose Sensor Applications

Muslima Zahan [1], Jiban Podder [1,*]

[1] Department of Physics, Bangladesh University of Engineering and Technology, Dhaka-1000, Bangladesh
* Correspondence: jpodder59@gmail.com (J.P.);

Scopus Author ID 9235115900

Received: 28.07.2021; Revised: 28.09.2021; Accepted: 5.10.2021; Published: 18.11.2021

Abstract: Nanostructured cobalt oxide (Co_3O_4) and Cu-doped Co_3O_4 thin films were synthesized by a simple spray pyrolysis technique at 450°C substrate temperature onto the plain glass substrate. The surface morphological, structural, optical, electronic, and glucose sensing effects of the deposited thin films were explored. Scanning Electron Microscope (SEM) images revealed a uniform, dense and porous surface morphology of Co_3O_4 and Cu doped Co_3O_4 thin films. X-ray diffraction (XRD) pattern showed the spinel cubic structure of lattice parameters a = b = c = 8.0764 Å and well agrees with the JCPDS card file no. 42-1467. The crystallite sizes were calculated as 29, 27, 24, and 26 nm with the variation of 0, 2, 4, and 6 % Cu doping concentrations, respectively. The obtained optical band gaps were about 2.02, 2.00, 2.09, and 1.98 eV for 0, 2, 4, and 6 % Cu doped Co_3O_4 thin films. The glucose sensing properties revealed that Cu doping greatly improved the sensing properties of Co_3O_4 thin film, and the highest glucose sensitivity was found at about 43%, and fast response time was about 0.97 sec at 4 % Cu doped Co_3O_4 thin-film.

Keywords: thin-film; nanostructure; Cu doped Co_3O_4; SEM; XRD; glucose sensitivity.

1. Introduction

Glucose plays an important role in human lifeblood. Frequently and accurately detection of glucose is of considerable sense in life. Glucose sensing for diabetes monitoring is crucial because it is a chronic disease that may cause death. Thus, due to the importance of glucose on the side of remedies, biotechnology, nutrition, and environmental science, the study of glucose detection has drawn tremendous attention [1, 2]. Among numerous metal oxides, the transition metal and spinel structures have drawn more interest in sensing abilities in many fields like catalysis, optoelectronic devices, magnetic data storage, biomaterials, electronics, bio/gas sensors, etc. [3-5]. Spinel cubic Co_3O_4 is one such family of metal oxide that carried out expanded passion because of its diverse properties and wide applications in the development of biosensors. From an application point of view, Cu doped Co_3O_4 (Cu: Co_3O_4) plays an essential aspect in catalysis and sensing performance. Distinct multiple oxidation states, structural variations, and elusive distribution of cations are maintained to prepare Cu: Co_3O_4. At low Cu concentration, lattice distortion would not be prominent, and the Cu enriched cubic spinel may observe while high Cu content tends to form an unstable phase. The sensing performance of spinel oxides in the middle of biosensors needs to improve by tailoring the precursor concentration, effective surface area, electron transfer properties, and material

biomolecule interface through morphology engineering [6, 7]. Till today substantial developments are attained in the controlled synthesis of Co_3O_4 thin films, and extended efforts have been given to synthesize Co_3O_4 and Cu: Co_3O_4 thin film beyond chemical bath deposition [8], sputtering [9], spray pyrolysis [10,11], pulsed laser deposition [12], chemical vapor deposition [13], sol-gel [14], dip coating [15] and hydrothermal method [16]. Among these various deposition techniques, the spray pyrolysis deposition technique is suitable because of its simplicity, ease to control, low cost, and scope of large area deposition. Very few reports are available in the literature on optical, structural, and electrical properties of Cu doped Co_3O_4 (Cu: Co_3O_4) thin films for glucose sensing performance. The aim of this work is to find out the surface morphological, structural, optical, and electronic properties of Co_3O_4 thin films synthesized via the spray pyrolysis method and to see the effect of copper doping concentrations on the suitability of glucose sensitivity measurements.

2. Materials and Methods

Cu: Co_3O_4 thin films were synthesized by a spray pyrolysis technique. The analytical grade cobalt acetate tetrahydrate [$Co(CH_3COO)_2{\cdot}4H_2O$] (Mark, 99%) and [$Cu(CH_3COO)_2{\cdot}H_2O$] (Mark, 98%) were used as mother precursor for Co and Cu sources, respectively. Deionized distilled water was used as a solvent. Ethanol (C_2H_5OH) and hydrochloric acid (HCl) were used as a reagent to control the pH value. The plain glass slide of area 5 × 2.5 cm^2 with a suitable mask was used as a substrate. The compressed dry air was used as a carrier gas. D-glucose ($C_6H_{12}O_6$) and sodium hydro oxide (NaOH) were used as precursors for sensitivity measurements.

The substrates were cleaned with acetone and distilled water in an ultrasonic cleaner for 30 min and subsequently dried in flowing hot air to execute a better adherence in the middle of the film and the substrate. In a typical procedure, 0.1 M aqueous solutions of $Co(CH_3COO)_2{\cdot}4H_2O$ mixed with different percentages (0-6 %) of $Cu(CH_3COO)_2{\cdot}H_2O$ was prepared in 100 mL of double-distilled water, including a few drops of C_2H_5OH and the mixed solvent was stirred about 1 h to form a clear homogeneous solution. After that, the solution was filtered and then sprayed through a fine bore in the form of fine droplets on pre-heated commercial glass substrates with a deposition time of 20 min. The deposition process was carried out at a 450°C constant substrate temperature. The substrate was put at a 25 cm distance from the spray nozzle. The air pressure was controlled by 0.5 bar as the carrier. 0.5 mL solution was maintained per minute as the spray rate throughout the experiment. The deposited thin films were allowed to cool at room temperature. The as-deposited Co_3O thin films were found homogeneous and dark brown. The possible chemical reaction during spray pyrolysis deposition is as follows:

$$(1\text{-}x)\ Co\ (CH_3COO)_2.4H_2O + x\ Cu\ (CH_3COO)_2.H_2O + H_2O + C_2H_5OH \rightarrow Co_{(3-x)}Cu_xO_4 \downarrow + CO_2 + CH_4\uparrow + H_2O\uparrow + H_2\uparrow$$

The surface morphology of Cu: Co_3O_4 films was studied by scanning electron microscope (SEM), Model: JSM-7600F operated at 20 kV. Structural properties were recorded by using a powder X-ray diffractometer (model: PANalytical Empyrean series 2, using CuKα radiation, λ = 1.54056 Å), with a diffraction angle between 10° to 90°. The crystallite size was determined from the broadening of corresponding X-ray spectral peaks by using Debye-Scherer's formula. Optical characterization of the films was carried out over 200–1100 nm wavelength by a UV-2600, Pc: UV–VIS–NIR; Shimadzu, double beam spectrophotometer.

Electrical measurements were carried out by the four-probe method. Glucose sensitivity was measured by an electrical method.

3. Results and Discussion

3.1. Surface morphology.

The SEM micrograph of undoped and 2, 4, 6 % Cu doped Co_3O_4 thin films are presented in Figure 1(a-d), respectively. All the images show that the substrates are uniformly covered with oxides. The surface morphology for pure Co_3O_4 is displayed in Figure 1(a) reveals the porous cobalt oxides layer, which may be due to the evolution of O_2 during decomposition at high temperature (450^{o}C). After 2 % Cu doping, the surface becomes smooth and compact because the macro defects are reduced due to a low Cu doping level shown in Figure 1 (b).

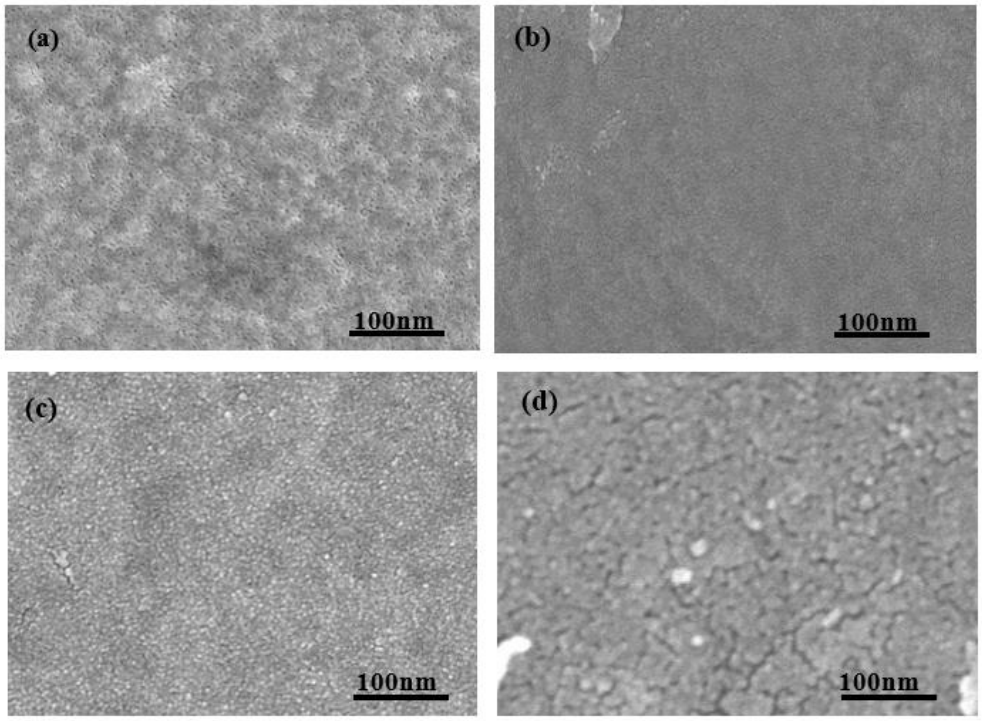

Figure 1. SEM micrograph of (a) Undoped Co_3O_4, (b) 2 % Cu doped Co_3O_4, (c) 4 % Cu doped Co_3O_4, (d) 6 % Cu doped Co_3O_4 thin films.

The reduction of macro defects is caused due to Cu doping as well as a smaller ionic radius of Cu ions in comparison with Co. The smaller Cu ions may occupy the different Co lattice sites, interstitial locations, and at the surface of the agglomerated particles. There is also a reduction of the oxygen vacancies due to the presence of Cu ions with +1 or +2 oxidation states. Figure 1(c) shows relatively homogeneous particle sizes and distribution for 4 % Cu concentration. Again, at 6 % Cu concentration demonstrated in Figure 1(d), the surface becomes more porous and rough because of a high amount of incorporated Cu, Cu^{2+} ions enter into the spinel Co_3O_4 lattice until stoichiometric [17].

3.2. Structural properties.

Figure 2 exhibited the XRD spectra of Cu: Co_3O_4 films at different Cu concentrations of 0, 2, 4, and 6 %, respectively. All of the diffraction peaks were perfectly indexed corresponding to the (220), (311), and (440) reflection planes at $2\theta = 31.30°$, 36.81°, and 65.20°

respectively and assigned to a pure spinel cubic phase of Co_3O_4 with a lattice constant of 8.0761 Å according to the (JCPDS file No 42-1467) [18]. The incorporation of the Cu atom strongly modifies the growth of the preferential orientation (311) plane. At a higher doping level of 6 %, the crystallinity is raised for the super-saturation of Cu atoms into the Co_3O_4 matrix. The peaks become sharper at a higher Cu concentration, indicating a larger grain size favorable for accumulating many charges over the surface.

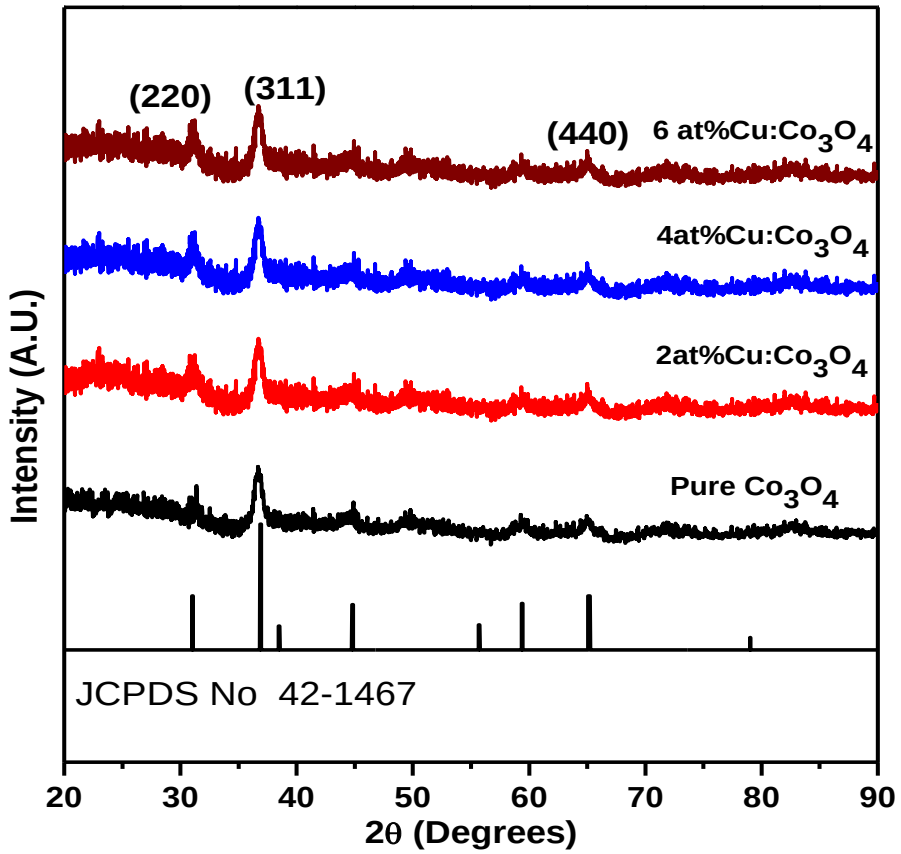

Figure 2. XRD pattern of pure and 2,4,6 % Cu doped Co_3O_4 thin films.

The preferred orientation peak (311) was observed at 36.81. No other peaks associated with the impurity phase were found with the increase of Cu concentrations, indicating that the phases are stable and Cu ions are uniformly incorporated within the Co_3O_4 lattice. The average crystallite size of Co_3O_4 thin film was estimated by using the classical Scherer's formula; $D = 0.89\lambda/\beta Cos\theta$ to the major peaks of diffraction spectrum where, β is full width at half maxima intensity of (311) plane, k = 0.89 is Scherrer constant, λ is X-ray wavelength used, and θ is diffraction angle and D is crystallite size. The calculated crystallite sizes decreased up to 4 % Cu and then increased [19]. This variation may lead to the substitution of tetrahedral Cu^{2+} cations and the creation of nanostructured poly-crystalline Cu-doped Co_3O_4, which may be favorable for accumulating a large number of charges over the surface of the films. The overall decrease in the crystallite size would also explain the surface-active area enhancement in copper-substituted Co spinel's. In a copper-cobalt mixed oxide system, the Co^{2+} ions are partially substituted by Cu^{2+} ions. The rise in Cu contents contributes to building up the evolution of octahedral Cu^{2+} and reducing the formation of octahedral Cu^{+}.

If Cu^{2+} ions and octahedral Co^{3+} ions are present in the copper-cobalt oxide system, then the oxide could be represented by $Cu^{2+}Co_2^{3+}O_4$, a form of copper-cobalt oxide structure as the 6 % Cu:Co_3O_4 films contains the higher number of Cu^{2+} ions which are not incorporated into copper-cobalt spinel structure compared with the 2 and 4 % Cu:Co_3O_4 films. The values

of the lattice parameter calculated from the (311) reflection plane are found to be a = 8.0764 Å. This value of lattice parameter, 'a' is found to be very close to the reported value of 8.084 Å from JCPDS for pure Co_3O_4 phase with cubic spinel symmetry and was found to increase with increasing Cu concentration. Also, dislocation density is defined as the dimension of dislocation per unit volume correlated to the density of defects in the sample and denoted by delta, δ which is calculated by the formula $\delta = \frac{1}{D^2}$. The texture coefficient, TC_{hkl} was specified to appraise the XRD results. The value of the texture coefficient point out a sample with inconstantly adapted crystallite and is calculated by,

$$TC_{hkl} = \frac{I_m\,(hkl)/I_s(hkl)}{n^{-1}\sum_n I_{m(hkl)}/I_{s(hkl)}}$$

where, TC (hkl) is the texture coefficient, I_m (hkl) is the measured intensity measured, Is (hkl) is standard intensity and n is total peak numbers. Variations of structural parameters with Cu contents are highlighted in Table 1. An increment in the lattice constant 'a' is observed as the amount of Cu doping concentration is increased. This result can be explained by taking into account the ionic radius of copper and cobalt in different coordination sites (0.73 Å and 0.62 Å for Cu^{2+} in octahedral and tetrahedral coordination, respectively, against 0.65 Å and 0.57 Å for Co^{2+} at low-spin octahedral sites and tetrahedral sites, respectively).

Table 1. Structural parameters of Cu: Co_3O_4 thin films.

Cu concentrations (%)	Lattice constant, a (Å)	Average crystallite size, D (nm)	Dislocation density 1/ δ^2 x 10^{-3} (lines/nm^2)	Texture coefficient, TC_{hkl}
0	8.0764	29	1.189	0.953
2	8.0836	27	1.372	0.999
4	8.0897	24	1.736	1.009
6	8.0953	26	1.479	1.036

Then, the increase in the unit cell parameter indicates a substitution of the cobalt by copper, although it cannot be ascertained whether Cu^{2+} occupies octahedral sites, tetrahedral sites, or both of them in the pristine cobalt oxide.

Dislocation densities show off aberration upon raising dopant concentrations. From table 1 we notice that when D decrease at 2 and 4 % of Cu doping concentration, the dislocation increase and suggests that defects in the Co_3O_4 matrix were generated by Cu, leading to a decrease in the crystallinity due to the formation of stress, a contraction of lattice because of substitution of the cobalt by copper. But at 6% Cu D increase, and the dislocation decreases because of improving crystallinity. Thus, in the present investigation, the variations of texture coefficient with Cu doping concentration showed randomly oriented crystallites for 4 % Cu presenting TC_{hkl} = 1.009 (~1).

3.3. Optical properties.

The optical parameters are the key factor in determining the quality of the prepared thin films and their suitability for biosensing applications. The optical absorbance of Co_3O_4 films is influenced by several factors, e.g., surface roughness, porosity, photogenerated electron-hole carriers. Figure 3 (a) depicts that absorbance increase with Cu concentration up to 4 %. The absorbance peaks obtained near 400 nm and 700 nm are for the transition among $O^{2-} \rightarrow Co^{2+}$ and $O^{2-} \rightarrow Co^{3+}$. Also, the absorbance band near 1000 nm may be assigned to the charge

deportation system in $Co^{2+} \leftrightarrow Co^{3+}$. The low absorbance in the NIR region than the visible region suggests that Co_3O_4 thin films are favorable for biosensing applications [20].

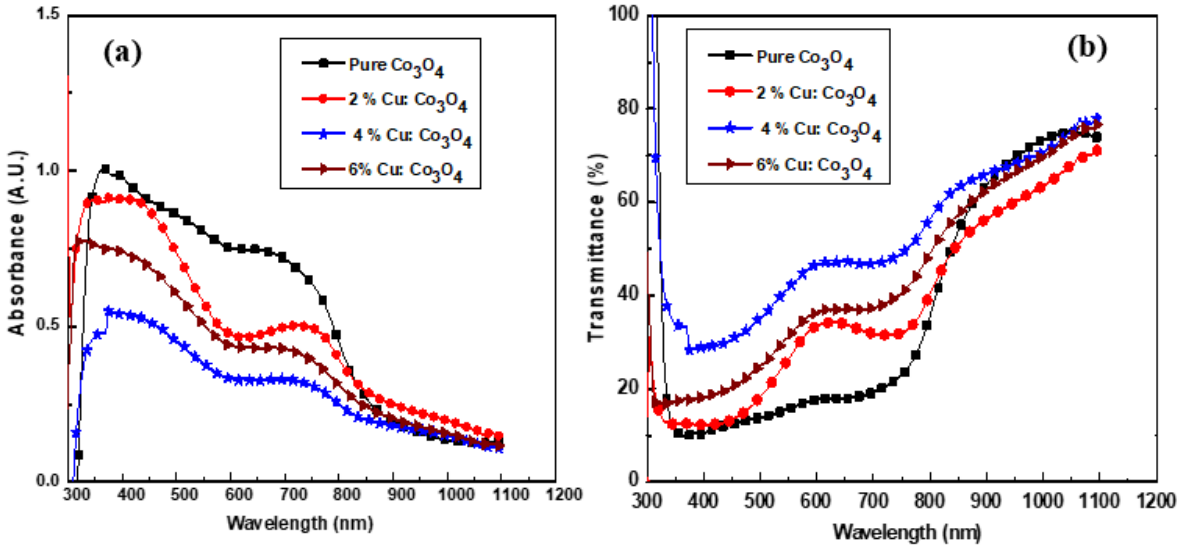

Figure 3. (a) wavelength vs. absorbance spectra (b) wavelength vs. transmittance spectra of Co_3O_4 variation with Cu concentration of 0, 2, 4, and 6%.

Figure 3 (b) displays wavelength vs. transmission spectra of Cu-doped Co_3O_4 thin films. In the vis-region, two sharp absorption edges were observed to lead the charge transfer event of ($O^{-2} \rightarrow Co^{2+}$) and ($O^{-2} \rightarrow Co^{3+}$) in Co_3O_4. In the IR region, high transmittance was obtained from 60% - 75%, highlighted in Figure 3 (b), which may be for structural homogeneity. There are no interferences within IR region (800 nm – 1100nm), indicating the films prepared are smooth and uniform.

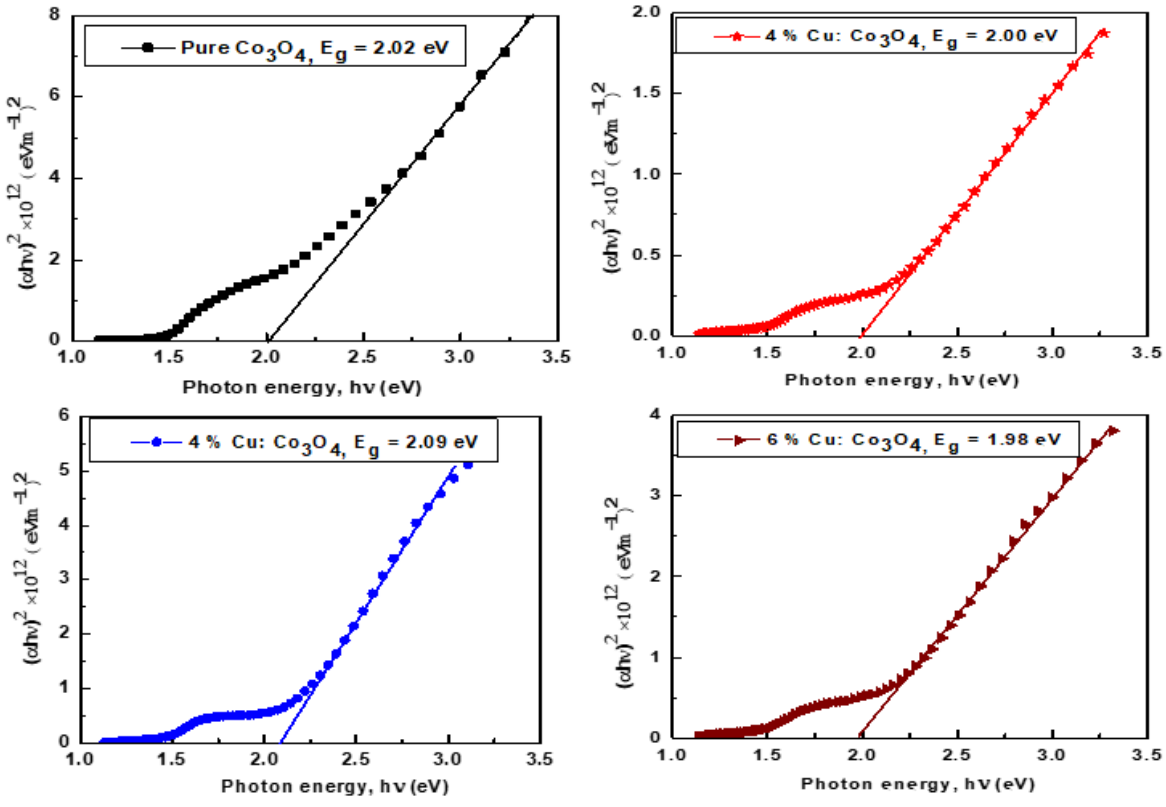

Figure 4. Taue plot of Co_3O_4 and Cu: Co_3O_4 thin films for 2,4 and 6 % Cu concentration.

This behavior may be for surface effect, better crystallinity, less surface irregularity, defect density, and $Co^{2+} \leftrightarrow Co^{3+}$ transition. Since Co_3O_4 (i.e., Co^{2+} $[Co^{3+}]_2O_4$) has a normal spinel crystal structure, the Co^{2+} ions take up the tetrahedral sites, while Co^{3+} ions employ the octahedral sites. As p states and d states are very close with each other, a transition may occur easily by p electrons resulting in a doublet corresponding to $O^{2-} \rightarrow Co^{3+}$ and $O^{2-} \rightarrow Co^{2+}$. The optical transmittance of nanostructured Cu: Co_3O_4 in the Vis-NIR domain comes mainly against Co ions' d–d, s–p, and p–d transitions.

The energy bandgap for various transitions in Co_3O_4 thin films has been calculated in our published article [21]. In this research work, Tauc relation: $\alpha = A/ h\nu (h\nu - E_g)^{1/2}$; where, E_g is bandgap, hν represents photon energy and A constant, was used to calculate ban gap. The plots of (hν) vs. $(\alpha h\nu)^2$ for Cu doped Co_3O_4 films displayed in Fig. 4 represent a linear section showing a direct bandgap of the films. Bandgap variation is slightly seen in Cu doped Co_3O_4 due to Cu concentration.

The maximum bandgap for 4% Cu is assigned to valence to conduction band excitation ($O^{2-} \rightarrow Co^{3+}$ charge transition), while the minimum bandgap is assigned to $O^{2-} \rightarrow Co^{3+}$ charge transfer for 6% Cu content. Where Co^{3+} ions are found below the conduction band; as a result, impurity energy levels are created within the bandgap. Contrarily, Cu contributes to the creation of holes and increases its role by the number of charge carriers (holes), which contribute to the conductivity knowing p-type Co_3O_4. The bandgap energy (E_g) of 0, 2, 4, and 6 %. Plotting $(\alpha h\nu)^2$ versus photon energy (hν) given the direct allowed transition presented in Fig. 5 also indicates p-type Cu: Co_3O_4 . It is observed that the bandgap slightly changed due to the effect of Cu concentration, and the maximum band gap was obtained at 4% Cu concentration. This behavior is caused by the distortion caused by Cu ions generating impurity energy levels within the bandgap of Co_3O_4 [22, 23].

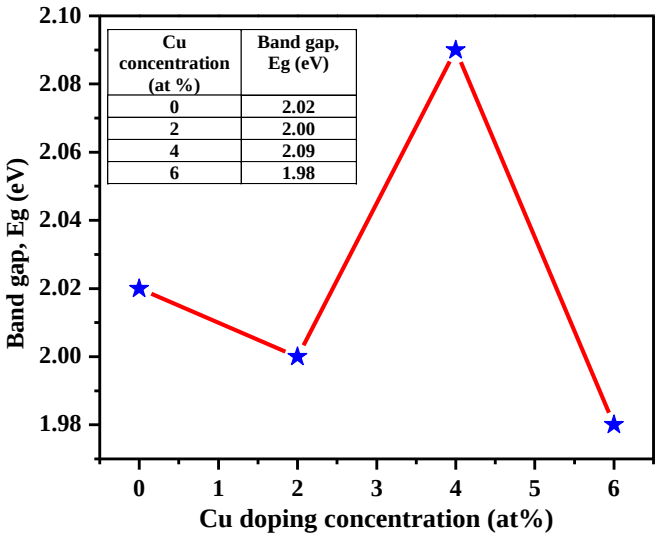

Figure 5. The bandgap of Cu: Co_3O_4 varying with Cu concentration of 0, 2, 4, and 6 at. %.

3.4. Electonic properties.

The change in electrical resistivity upon temperature ranging from 320 - 400 K for Co_3O_4 and 2, 4, and 6 % Cu doped Co_3O_4 thin films are shown in Figure 6 (a). It is noticed that the resistivity decreases with the temperature rise. This type of variation indicates the semiconducting behavior of the films. The decrease in resistivity may be attributed to the increase of the acceptor states associated with the integration of Cu impurities into Co sites of

the Co_3O_4 lattice. Cu is a popular acceptor dopant with good electrical conductivity, which increases the hole concentration inter valence band at room temperatures. In the presence of Cu doping, the inter-grain boundary area reduces, and there is a decreasing tendency in the electron scattering. This results in the reduction of resistivity. Figure 6(b) shows the change in conductivity due to the effect of Cu concentration. Hall mobility and carrier concentration also change with the rise of Cu concentrations in Cu-doped Co_3O_4 thin films. It may be due to the effect of low energy barrier height on the carriers, which logically increases with an increase of the amount of dopant and subsequent improvement of charge density [24]. Table 2 records the electronic properties of the Cu: Co_3O_4 thin films deposited at 0, 2, 4, and 6 % Cu concentration. Therefore, based on the carrier concentration values listed in Table 2, it can be concluded that the number of Cu vacancies increases with increasing the Cu concentration, resulting in a higher hole carrier concentration. However, it can be seen an increase in the mobility and reduction in the carrier concentration might be due to the lower rate of Cu, which can lead to a better crystallinity and reduce the number of glitches in the lattice of the deposited film. Table 2 shows the minimum Hall mobility (μ) at 4% Cu concentration which may agree with the shortening of the effective mean free path of conduction carriers by scattering from the film's surface when Cu is doped into Co_3O_4. It is bound that an expansion of charge carrier upon the raise of Cu dopant is apparently for the generation of more acceptor levels within Co ions as the Cu ions demand to be half-filled free electron from its outer shell. The variation of Hall mobility is mainly due to the increase of carrier concentration and high electrical conductivity.

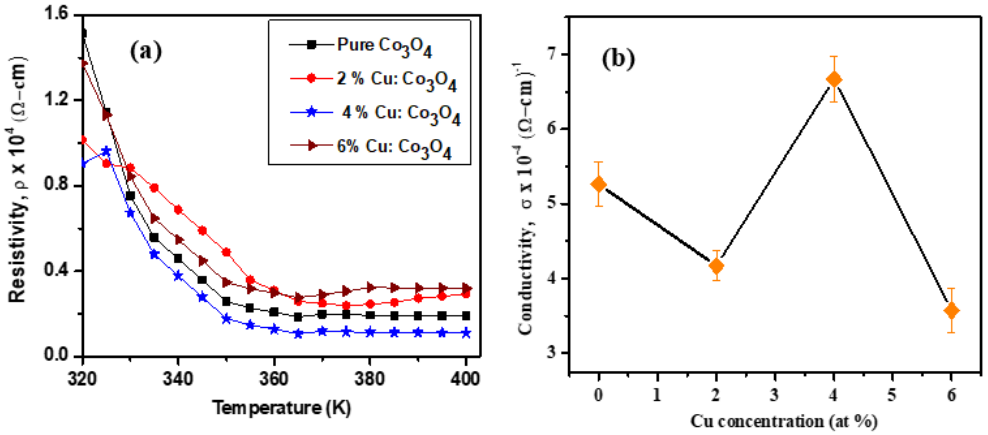

Figure 6. (a) Variation of electrical resistivity with temperature (b) Variation of electrical conductivity with Cu concentration of 0, 2, 4, and 6%.

Table 2. Electrical parameters of Cu: Co_3O_4 thin films variation with Cu concentrations.

Cu concentration (%)	Resistivity, ρ ($\times 10^4$ Ω-cm)	Carrier concentration, n ($\times 10^{17}$ cm^{-3})	Hall mobility, μ ($cm^2 V^{-1} s^{-1}$)
0	0.23	2.39	1.81
2	0.27	2.86	2.15
4	0.15	3.13	1.97
6	0.28	3.82	2.39

3.5. Glucose sensing performance.

3.5.1. Experimental procedure.

The sensing of bio components and chemical species is increasing significantly nowadays. In the case of chemical species sense, it is essential to distinguish sensing devices that are crucial to simplify a better life. Diabetes mellitus is the major cause of death and

disability in the world. It is effectively controlled by regular monitoring of physiological blood glucose levels. Traditional glucose sensors are enzymatic microsensors, which utilize glucose oxidase (GOx) on the film surface to oxidize glucose. The main point of view is to oxidize glucose on the electrode surface without any enzyme. Nanostructured Co_3O_4 is more suitable for antisemitic glucose sensors as it possesses good catalytic properties, enormous surface area, and fast electron transfer, making the ideal detection elements like glucose.

The sensing abilities of pure Co_3O_4 and 2,4 and 6 % Cu: Co_3O_4 thin films concerning glucose ($C_6H_{12}O_6$) were evaluated by the four-probe method. The schematic diagram of the four-probe methods for glucose sensing is shown in Figure 7.

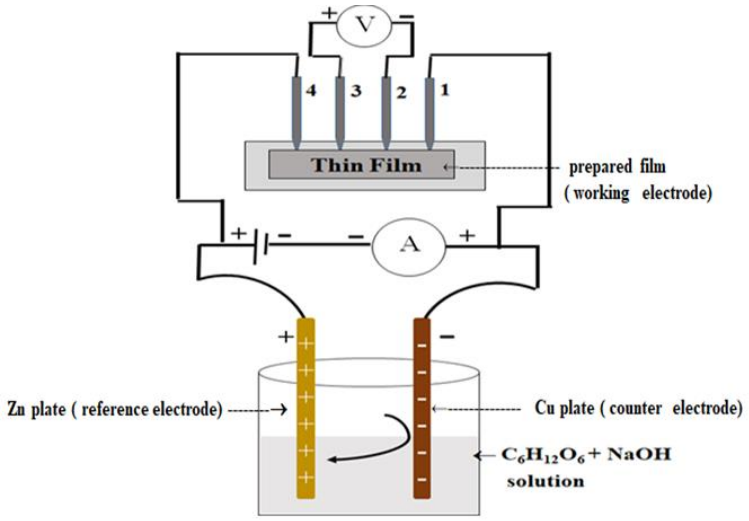

Figure 7. Schematic diagram of four-probe methods for glucose sensing.

In this study, 0.2 M $C_6H_{12}O_6$ (3.62gm) and 0.2 M NaOH (0.8gm) were dissolved into 200 ml distilled water. NaOH usually coexists with glucose. The precursors have been stirred for about 1 hour with a magnetic stirrer to have a homogeneous glucose concentration. A constant supply voltage of + 65V was applied for the sensitivity measurement. Two electrodes, one is as a reference (positive electrode), and another is as a counter (negative electrode), were put into the prepared solution, which was connected with an ammeter and probes of the four-probe system. The synthesized thin film was appointed under four probes which work as working electrodes (anode). Sensitivity of pure Co_3O_4 and 2, 4, and 6 % Cu doped Co_3O_4 thin films were measured by measuring current variation with time, keeping constant glucose concentration by the selected method. The rapid electron trance between the Co_3O_4 layer and the substrate may cause to enhance the sensing ability means that the key factor in enhancing sensing ability is a fast electron transfer between the Co_3O_4 layer and the substrate to improve electron collection.

Likewise, glucose sensing depends on the air oxidation of glucose molecules on the surface of the film layer and decomposition into gluconolactone ($C_6H_{10}O_6$) and hydrogen peroxide (H_2O_2). Prominently, on the surface of the deposited films, oxidation of glucose molecules consequence hydrogen peroxide, which passes through the porous thin film and is adsorbed on the surface layer. Due to the oxidation-reduction of hydrogen peroxide molecules, the surface area increases the reaction speed and the output current. In the time being exerted, NaOH was used in the $C_6H_{12}O_6$ solution for increasing current to reach a stable state as glucose and OH^- molecules are adsorbed in the film surface. The possible chemical reactions are given as:

$$C_6H_{12}O_6 + H_2O + O_2 \rightarrow C_6H_{10}O_6 + H_2O_2$$
$$H_2O_2 \rightarrow O_2 + 2H^+ + 2e^-$$
$$NaOH \rightarrow Na^+ + OH^-$$
$$C_6H_{12}O_6 + H_2O + NaOH \rightarrow C_6H_{10}O_6 + O_2 + H^+ + 2e^-$$

The electrons produced in those reactions are transferred through the film layer.

3.5.2. Measurement of the sensing current.

The rapid rise in current was observed concerning time to influence a steady state. The sensing current was pulled off at constant supply voltage with time for different Cu concentrations. The current-time response for pure and Cu: Co_3O_4 thin films are displayed in Figure 8 (a-d). In ascertained, the rise of sensing current is observed for Cu contents, and the maximum current response is obtained at 4 % Cu doping. The reason is for the interactivity of atoms from solution onto the highly textured and dense film surface. The oxygen ions may interact immediately on the film surface at the film surface, bonding with $C_6H_{12}O_6$ molecules. This fast interaction provides considerable charge carriers responsible for the sensing current's tapering rise [25].

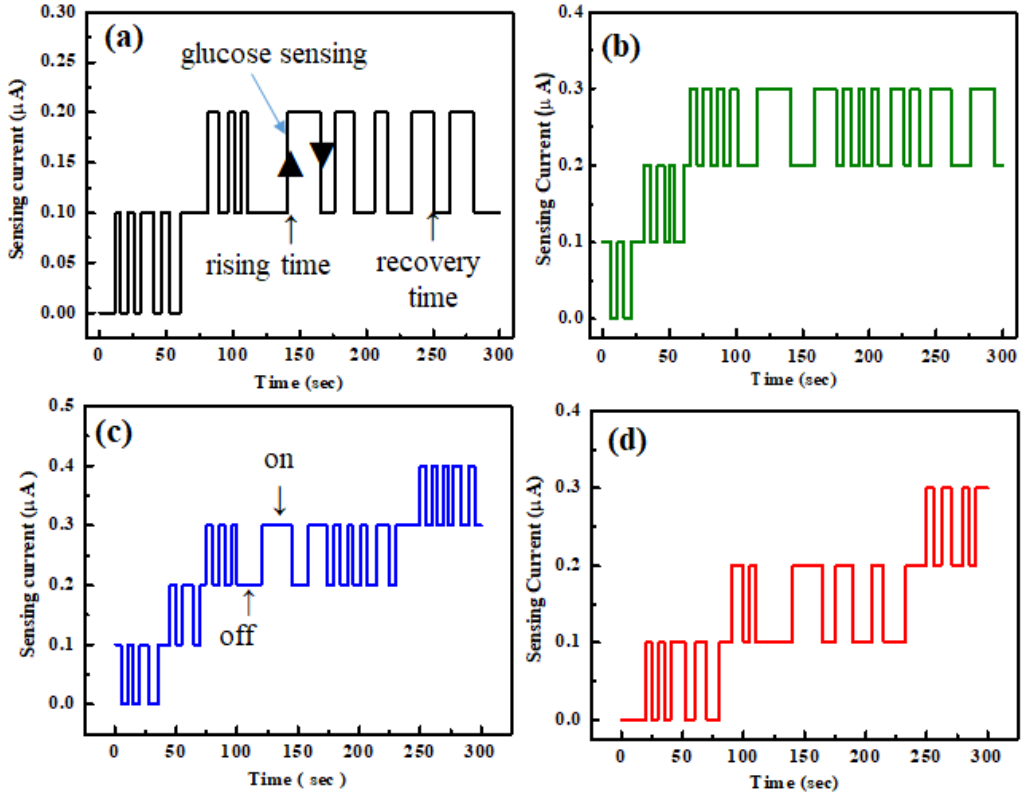

Figure 8. Current-time response plot (a) pure Co_3O_4 (b) 2 % Cu: Co_3O_4 (c) 4 % Cu: Co_3O_4 (d) 6 % Cu: Co_3O_4 thin films.

The rectangular response of Fig.8 indicates the edged rise of current with time reaching a stable. In our study, no other species were used except glucose to detect. Hence, Cu-O-Co bonds formed at the substrate interface and the films, which probably facilitates electrons transfer across the interface to cause a high current response. This result agrees with the other published work [26,27], where they used other species, i.e., sucrose, uric acid, ascorbic acid, etc., with glucose.

3.5.3. Sensitivity measurements.

Glucose-sensing ability of the deposited thin films was determined using the following relation [16]

$$S = \left(\frac{I_a - I_g}{I_g}\right) \times 100$$

Where I_a indicates the current in the air and I_g represents the current-carrying glucose. Figure 9 (a) shows the glucose response of pure and Cu: Co_3O_4 thin films with Cu concentration and time variation. The response was dramatically increased with the increase of Cu concentration, especially for 4 % Cu higher than others shown in Fig. 9 (b), which may be due to smaller crystallite size and higher bandgap. The sensitivity of the thin films prepared in this study is higher than those in previous reports of spin-coated or electrodeposited Co_3O_4 films [28,29]. The selectivity data are given in Table 3.

Table 3. Selectivity data variation with Cu concentration.

Cu concentration (%)	Glucose response time (Sec)	Glucose sensitivity (%)
0	1.15	22
2	1.09	18
4	0.97	43
6	1.03	33

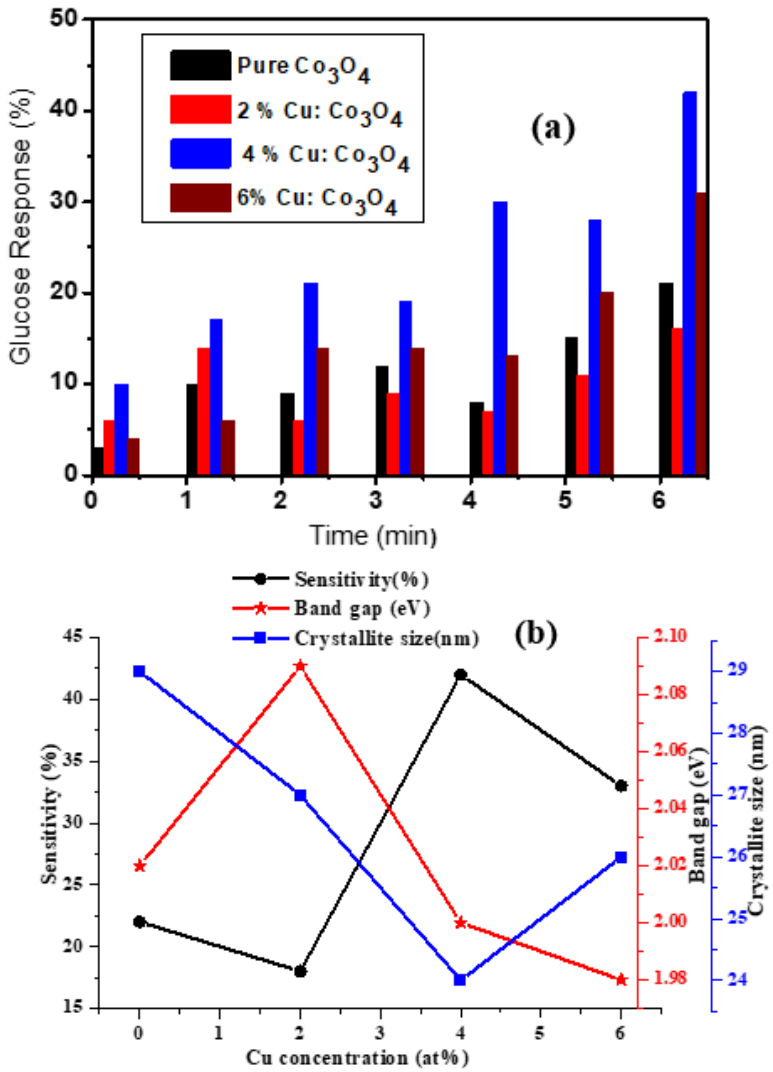

Figure 9. (a) Glucose response of pure and Cu: Co_3O_4 thin films variation with Cu concentration and time (b) Correlation of sensitivity, crystallite size, and bandgap with Cu concentration.

In this paper, the effect of Cu doping concentration on the Co_3O_4 sensibility is investigated. In particular, 4 % Cu: Co_3O_4 films shows a fast response time (0.97s) and high sensitivity (43%) than other samples shown in Table 3 and Figure 9(b). This may be for the deactivation of the shallow sphere of Co_3O_4 with 6 % Cu doped samples. This increases the electron concentration, which eventually increases the oxygen vacancies-related defects in Co_3O_4 nanoparticles. Therefore, oxygen vacancies provide more adsorption sites for liquid molecules, causing the surface to become highly active for a reaction to improve the sensing properties. In different circumstances, low optical band gap and crystallite size displayed in Figure 9(b), which are responsible for the incorporation of Cu^{2+} ions into Co_3O_4 octahedral sites due to variation of the ionic radius, may be leading to form more oxygen vacancies, which improves glucose-sensing properties of Cu-doped Co_3O_4 thin films.

These results agree with other researchers [26] and our previous works [30,31]. Compared to other studies, the present work exhibited high sensitivity and low detection limit with reasonable response time. In the present work, we have measured rising and response time from the plot of time vs. sensing current (with glucose) displayed in Figure 10. The rising and response time characteristic curves based on the glucose-sensing performance show a change in current with time in seconds. The rising time of pure Co_3O_4 and 2, 4, and 6 % Cu doped Co_3O_4 thin films were found to be 117.89, 117.94, 118.05, and 117.97 sec respectively. The response times were 1.16, 1.09, 0.97, and 1.03 sec for pure and 2, 4, and 6 % Cu doped Co_3O_4 thin films, respectively. In addition to that, the fast response shows excellent stability in the developed sensor.

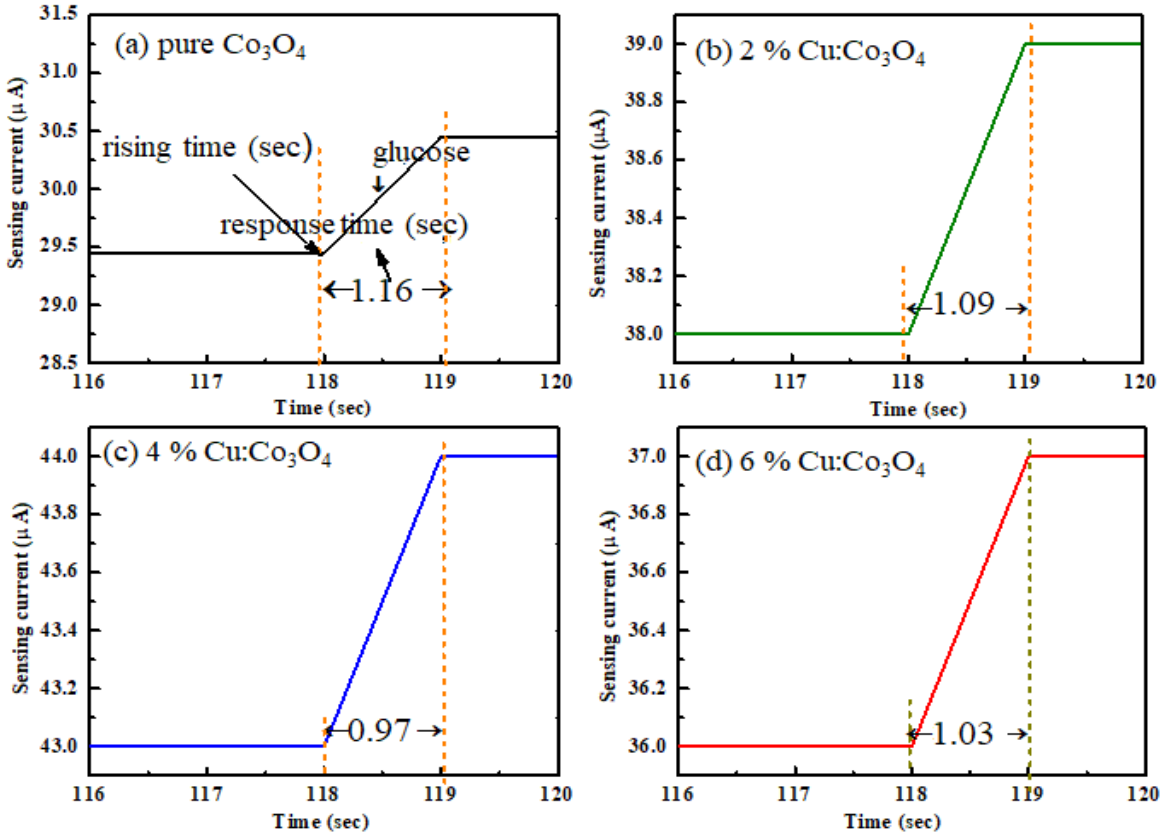

Figure 10. Response time of Cu: Co_3O_4 at 0, 2, 4, and 6 %. Cu concentration.

These results are in good agreement with other researchers [26] and our previous works [30,31]. Compared to other studies, the present work exhibited high sensitivity and low detection limit with reasonable response time. In the present work, we have measured rising

and response time from the plot of time vs. sensing current (with glucose) displayed in Figure 10. The rising and response time characteristic curves based on the glucose-sensing performance show a change in current with time in seconds. The rising time of pure Co_3O_4 and 2, 4, and 6 % Cu doped Co_3O_4 thin films were found to be 117.89, 117.94, 118.05, and 117.97 sec, respectively. The response times were 1.16, 1.09, 0.97, and 1.03 sec for pure and 2, 4, and 6 % Cu doped Co_3O_4 thin films. In addition to that, the fast response shows excellent stability in the developed sensor.

While the response time is measured from the plot of time vs. sensing current (with glucose) as displayed in Figure 10, response time less than 1 sec, e.g., 0.97, is calculated from the graph. Therefore, from our experiments, it can be concluded that 4 % Cu doped Co_3O_4 thin films may be more suitable for glucose sensing developments than other Cu concentrations.

4. Conclusions

Surface morphological, structural, optical, and electronic properties of pure Co_3O_4 and Cu-doped Co_3O_4 thin films synthesized using a spray pyrolysis technique with different Cu concentrations of 0, 2, 4, and 6 % are investigated. The surface homogeneity of the deposited films increases with Cu content belongings friction among the charge carriers. XRD patterns indicated that Cu ions substituted the Co ions without altering the structure. The particle size reduces from 29 to 24 nm by increasing Cu concentration from 0 to 4 %. The most prominent peak along the (311) plane are observed in both pure and Cu doped Co_3O_4 thin films. In the visible–near-infrared region, the films showed highly transparent, and the transmittance increases with the raising Cu concentration at 4 % and reaching a maximum of 75%. The direct bandgap energy of the films varies between 1.98 to 2.09 eV upon Cu consents. Small crystallite size, the regularity of surface morphology, high transmittance, and tunable bandgap, high conductivity of Cu doped Co_3O_4 thin films suggest the suitability of the material in optoelectronic devices and biosensing applications. Moreover, small crystallite size, the regularity of surface morphology, less resistivity, high carrier concentration obtained at 4 % Cu doped Co_3O_4 thin films could be suitable for optoelectronic and biosensing devices.

In conclusion, it is demonstrated that Cu-doped Co_3O_4 thin film could be a favorable nanostructured biomedical sensor for glucose ($C_6H_{12}O_6$) response. The highest sensing abilities have been obtained for 4 % Cu doped Co_3O_4. Spray deposited Co_3O_4 and Cu: Co_3O_4 thin films give the high specific surface stretch of the film layer and its firm adhesion to the substrate, which consecutively afford to the admirable sensing performance of the prepared films.

Funding

This research received no external funding.

Acknowledgments

The authors would like to express their cordial thanks to the spray pyrolysis lab of the Department of Physics of Bangladesh University of Engineering and Technology for providing necessary laboratory support. One of the authors, Muslima Zahan, is grateful to the Ministry of Science and Technology, Government of the People's Republic of Bangladesh, for granting NST fellowship to carry out the Ph.D. program. This publication is dedicated to the birth centenary of the Father of the Nation of Bangladesh 'Bangabandhu Sheikh Mujibur Rahman'.

Conflicts of Interest

The authors declare no conflict of interest.

References

1. Hartono, A.; Sanjaya, E.; Ramli, R. Glucose Sensing Using Capacitive Biosensor Based on Polyvinylidene Fluoride Thin Film. *Biosensors* **2018**, 30;8(1):12, http://doi.org/10.3390/bios8010012.
2. Marie, M.; Mandal, S.; Manasreh, O. An Electrochemical Glucose Sensor Based on Zinc Oxide Nanorods. *Sensors* **2015**, *15*, 18714-18723, https://doi.org/10.3390/s150818714.
3. Jincy, C.S.; Meena, P. Synthesis of Cu doped cobalt oxide nanoparticles as ammonia gas sensor operating at room temperature. *Materials Today: Proceedings* **2021**, *43*, 2459-2463, http://doi.org/10.1016/j.matpr.2021.02.529.
4. Jadhav, S.B.; Malavekar, D.B.; Kale, S.B.; Sabale, S.R.; Patil, U.M.; Lokhande, C.D.; Pawaskar, P.N. Reliable glucose sensing properties of electrodeposited vertically aligned manganese oxide thin film electrode. *Applied Physics A* **2021**, *127(5)*, https://doi.org/10.1007/s00339-021-04544-3.
5. UmaSudharshini, A.; Bououdina, M.; Venkateshwarlu, M.; Dhamodharan, P.; Manoharan, C. Solvothermal synthesis of Cu-doped Co_3O_4 nanosheets at low reaction temperature for potential supercapacitor applications. *Applied Physics A* **2021**, *127(5)*, https://doi.org/10.1007/s00339-021-04498-6.
6. Li, C.; Han, X.; Cheng, F.; Hu, Y.; Chen, C.; Chen, J. Phase and composition controllable synthesis of cobalt manganese spinel nanoparticles towards efficient oxygen electrocatalysis. *Nature Communications* **2015**, *6*, http://doi.org/10.1038/ncomms8345.
7. Palmer, M.; Masikini, M.; Jiang, L.-W.; Wang, J.-J.; Cummings, F.; Chamier, J.; Inyang, O.; Chowdhury, M. Enhanced electrochemical glucose sensing performance of CuO:NiO mixed oxides thin film by plasma assisted nitrogen doping. *Journal of Alloys and Compounds* **2021**, *853*, https://doi.org/10.1016/j.jallcom.2020.156900.
8. Sengupta, S.; Kumar, A.; Jain, V.K. Cadmium Sulfide (CdS) Thin Films with Improved Morphology for Humidity Sensing by Chemical Bath Deposition at Lower pH. *Journal of Nanoscience and Nanotechnology* **2021**, *21*, 6035-6040, https://doi.org/10.1166/jnn.2021.19521.
9. Hippler, R.; Cada, M.; Ksirova, P.; Olejnicek, J.; Jiricek, P.; Houdkova, J.; Wulff, H.; Kruth, A.; Helm, C.A.; Hubicka, Z. Deposition of cobalt oxide films by reactive pulsed magnetron sputtering. *Surface and Coatings Technology* **2021**, *405*, https://doi.org/10.1016/j.surfcoat.2020.126590.
10. Athey, P.R.; Urban, F.K.; Tabet, M.F.; McGahan, W.A. Optical properties of cobalt oxide films deposited by spray pyrolysis. *Journal of Vacuum Science & Technology A* **1996**, *14*, 685-692, https://doi.org/10.1116/1.580372.
11. Dhamodharan, P.; Chen, J.; Manoharan, C. Fabrication of In doped ZnO thin films by spray pyrolysis as photoanode in DSSCs. *Surfaces and Interfaces* **2021**, *23*, https://doi.org/10.1016/j.surfin.2021.100965.
12. Farhad, S.F.U. The effect of substrate temperature and oxygen partial pressure on the properties of nanocrystalline copper oxide thin films grown by pulsed laser deposition. *Data in Brief* **2021**, *34*, https://doi.org/10.1016/j.dib.2020.106644.
13. Méndez-Lozano, N.; Apátiga-Castro, M.; Manzano-Ramírez, A.; Rivera-Muñoz, E.M.; Velázquez-Castillo, R.; Alberto-González, C.; Zamora-Antuñano, M. Morphological study of TiO_2 thin films doped with cobalt by Metal Organic Chemical Vapor Deposition. *Results in Physics* **2020**, *16*, https://doi.org/10.1016/j.rinp.2019.102891.
14. Mehmood, B.; Khan, M.I.; Iqbal, M.; Mahmood, A.; Al-Masry, W. Structural and optical properties of Ti and Cu co-doped ZnO thin films for photovoltaic applications of dye sensitized solar cells. *International Journal of Energy Research* **2021**, *45*, 2445-2459, https://doi.org/10.1002/er.5939.
15. Cathro, K.J. Preparation of cobalt-oxide-based selective surfaces by a dip-coating process. *Solar Energy Materials* **1984**, *9*, 433-447, https://doi.org/10.1016/0165-1633(84)90017-0.
16. Raba, A.M.; Julieta, L.; Flechas, C.; Joya M.R. Synthesis and evaluation of nickel doped Co_3O_4 produced through hydrothermal technique. *DYNA* **2020,** *87*, 184-191.
17. Amri, A.; Duan, X.; Yin, C.-Y.; Jiang, Z.-T.; Rahman, M.M.; Pryor, T. Solar absorptance of copper–cobalt oxide thin film coatings with nano-size, grain-like morphology: Optimization and synchrotron radiation XPS studies. *Applied Surface Science* **2013**, *275*, 127-135, https://doi.org/10.1016/j.apsusc.2013.01.081.
18. Cullity, B.D.; Stock, S.R. *Elementary of X-Ray Diffraction*. Third Edition, Prentice-Hall in the United States of America, **2001.**
19. Abu-Zied, B.M.; Bawaked, S.M.; Kosa, S.A.; Schwieger, W. Effect of microwave power on the thermal genesis of Co_3O_4 nanoparticles from cobalt oxalate micro-rods. *Applied Surface Science* **2015**, *351*, 600-609, https://doi.org/10.1016/j.apsusc.2015.05.151.
20. Farhan, M.; Khodair, Z.; Ibrahim, B. Study of the Structural and Optical Properties of Ni-doped Co_3O_4 Thin Films Using Chemical Spray Pyrolysis Technique. *IOP Conference Series: Materials Science and Engineering* **2020**, *871*, https://doi.org/10.1088/1757-899X/871/1/012090.

21. Zahan, M.; Podder, J. Surface morphology, optical properties and Urbach tail of spray deposited Co_3O_4 thin films. *Journal of Materials Science: Materials in Electronics* **2019**, *30*, 4259-4269, https://doi.org/10.1007/s10854-019-00717-2.
22. Pankove, J. *Optical Processes in Semiconductors*. Englewood Cliffs: Prentice-Hall **1971**.
23. Ali, G.A.M.; Fouad, O.A.; Makhlouf, S.A. Structural, optical and electrical properties of sol–gel prepared mesoporous Co_3O_4/SiO_2 nanocomposites. *Journal of Alloys and Compounds* **2013**, *579*, 606-611, https://doi.org/10.1016/j.jallcom.2013.07.095.
24. Li, Q.; Sun, X.; Lozano, K.; Mao, Y. Asymmetric supercapacitors with dominant pseudocapacitance based on manganese oxide nanoflowers in a neutral aqueous electrolyte. *RSC Advances* **2013**, *3*, 24886-24890, https://doi.org/10.1039/C3RA45140B.
25. Ding, Y.; Wang, Y.; Su, L.; Bellagamba, M.; Zhang, H.; Lei, Y. Electrospun Co_3O_4 nanofibers for sensitive and selective glucose detection. *Biosensors and Bioelectronics* **2010**, *26*, 542-548, https://doi.org/10.1016/j.bios.2010.07.050.
26. Mahmoud, A.; Echabaane, M.; Omri, K.; Boudon, J.; Saviot, L.; Millot, N.; Chaabane, R.B. Cu-Doped ZnO Nanoparticles for Non-Enzymatic Glucose Sensing. *Molecules* **2021**, *26*, http://doi.org/10.3390/molecules26040929.
27. Harry, M.; Chowdhury, M.; Cummings, F.; Arendse, C.J. Elemental Cu doped Co_3O_4 thin film for highly sensitive non-enzymatic glucose detection. *Sensing and Bio-Sensing Research* **2019**, *23*, https://doi.org/10.1016/j.sbsr.2019.100262.
28. Chowdhury, M.; Cummings, F.; Kebede, M.; Fester, V. Binderless Solution Processed Zn Doped Co_3O_4 Film on FTO for Rapid and Selective Non-enzymatic Glucose Detection. *Electroanalysis* **2017**, *29*, 578-586, https://doi.org/10.1002/elan.201600440.
29. Chowdhury, M.; Ossinga, C.; Cummings, F.; Chamier, J.; Kebede, M. Novel Sn Doped Co_3O_4 Thin Film for Nonenzymatic Glucose Bio-Sensor and Fuel Cell. *Electroanalysis* **2017**, *29*, 1876-1886, https://doi.org/10.1002/elan.201700184.
30. Zahan, M.; Podder, J. Role of Fe doping on structural and electrical properties of MnO_2 nanostructured thin films for glucose sensing performance. *Materials Science in Semiconductor Processing* **2020**, *117*, 105109, https://doi.org/10.1016/j.mssp.2020.105109.
31. Zahan, M.; Podder, J. Structural, optical and electrical properties of Cu:MnO_2 nanostructured thin films for glucose sensitivity measurements. *SN Applied Sciences* **2020**, *2:385*, https://doi.org/10.1007/s42452-020-2191-8.